

A&A manuscript no.  
(will be inserted by hand later)

Your thesaurus codes are:  
3(11.01.2; 11.19.3; 13.09.1)

ASTRONOMY  
AND  
ASTROPHYSICS

# Mid-infrared diagnostics to distinguish AGNs from starbursts <sup>\*</sup>

O. Laurent<sup>1,2</sup>, I.F. Mirabel<sup>1,3</sup>, V. Charmandaris<sup>4,5</sup>, P. Gallais<sup>1</sup>, S.C. Madden<sup>1</sup>, M. Sauvage<sup>1</sup>, L. Vigroux<sup>1</sup> and C. Cesarsky<sup>1,6</sup>

<sup>1</sup> CEA/DSM/DAPNIA Service d'Astrophysique F-91191 Gif-sur-Yvette, France

<sup>2</sup> Max-Planck-Institut für extraterrestrische Physik, Postfach 1603, 85740 Garching, Germany

<sup>3</sup> Instituto de Astronomía y Física del Espacio. cc 67, suc 28. 1428 Buenos Aires, Argentina

<sup>4</sup> Observatoire de Paris, DEMIRM, 61 Av. de l'Observatoire, F-75014 Paris, France

<sup>5</sup> Astronomy Department, Cornell University, Ithaca NY, 14853, USA

<sup>6</sup> European Southern Observatory, 85748 Garching, Germany

Received 1 June 1999 / Accepted 18 May 2000

**Abstract.** We present new mid-infrared (MIR) diagnostics to distinguish emission of active galactic nuclei (AGN) from that originating in starburst regions. Our method uses empirical spectroscopic criteria based on the fact that MIR emission from star forming or active galaxies arises mostly from HII regions, photo-dissociation regions (PDRs) and AGNs. The analysis of the strength of the 6.2  $\mu\text{m}$  Unidentified Infrared Band (UIB) and the MIR continuum shows that UIBs are very faint or absent in regions harboring the intense and hard radiation fields of AGNs and pure HII regions, where the UIB carriers could be destroyed. The MIR signature of AGNs is the presence of an important continuum in the 3-10  $\mu\text{m}$  band which originates from very hot dust heated by the intense AGN radiation field. Using these two distinct spectral properties found in our MIR templates, we build diagnostic diagrams which provide quantitative estimates of the AGN, PDR and HII region contribution in a given MIR spectrum. This new MIR classification can be used to reveal the presence of AGNs highly obscured by large columns of dust.

**Key words:** Galaxies: active – Galaxies: starburst – Infrared: galaxies

## 1. Introduction

Since the discovery by IRAS of ultraluminous infrared galaxies ( $L(8-1000 \mu\text{m}) > 10^{12} L_{\odot}$ ) which emit the bulk of their energy in the infrared, a large number of studies have shown that intense star forming regions as well as

AGNs are necessary to explain these high luminosities (see Sanders & Mirabel 1996 for a review). Large concentrations of molecular gas are needed for fueling nuclear starbursts and/or AGNs. Consequently, absorption makes the distinction between starburst and AGN activity difficult and the estimate of their relative contribution to the total infrared luminosity is far from straightforward. Optical classification (Veilleux et al. 1995, Goldader et al. 1995, Kim et al. 1998) is plagued by extinction, while radio wavelengths, although free from extinction, do not result in a definite classification (Condon et al. 1991, Lonsdale et al. 1993, Smith et al. 1998). Based on X-ray observations (Ogasaka et al. 1997, Risaliti et al. 2000), ground-based infrared observations (Roche et al. 1991, Dudley 1999, Murphy et al. 1999, Soifer et al. 2000) and on ISO observations (Genzel et al. 1998, Lutz et al. 1998, Rigopoulou et al. 1999), considerable progress has been made in defining the fraction of the AGN/Starburst contributions to the bolometric luminosity of ultraluminous infrared galaxies.

To further examine the AGN and starburst connection, we have observed a sample of nearby active and interacting galaxies harboring starburst regions and/or AGNs using ISOCAM. Due to the unique spectro-imaging capabilities of the camera which provide an angular resolution of 4-8 arcsec between 5 and 16  $\mu\text{m}$  (200-400 pc at 10 Mpc), we can reveal and study obscured central regions not visible at optical wavelengths ( $A_{15 \mu\text{m}} \sim A_V / 70$ , Mathis 1990).

The goal of this paper is to present an empirical method to distinguish and quantify the MIR emission coming from starbursts and AGNs. Our approach is based on a new MIR diagnostic for estimating the relative importance of these two main energy sources found in galactic centers. Our sample and the data reduction methods are described in section 2. A brief summary of the typical MIR emission encountered in these galaxies is presented in section 3, while our MIR templates and diagnostic dia-

*Send offprint requests to:* O. Laurent, olaurent@mpe.mpg.de

<sup>\*</sup> Based on observations made with ISO, an ESA project with instruments funded by ESA Member States (especially the PI countries: France, Germany, the Netherlands and the United Kingdom) and with the participation of ISAS and NASA.

arXiv:astro-ph/0005376v1 18 May 2000

grams are shown in section 4. We discuss our results and their implications in section 5 and the final conclusions are given in section 6.

## 2. Observations and data reduction

A large sample of nearby galaxies hosting star formation activity and AGN signatures (see Table 1) was observed with the ISOCAM camera (Cesarsky et al. 1996) on board the Infrared Space Observatory (ISO, Kessler et al. 1996). All observations come from the ISOCAM consortium guaranteed time programs and most of them were part of the active galaxy proposal CAMACTIV (P.I. I.F. Mirabel, e.g. Charmandaris et al. 1999, Mirabel et al. 1998, Gallais et al. 1998, Mirabel et al. 1999). These galaxies have been observed either in the spectro-imaging mode with the Circular Variable Filter (CVF) or in the raster mode with broad band filters.

The CVF covers a spectral range from 5 to 16  $\mu\text{m}$  with a spectral resolution of  $\sim 40$ . For CVF scans, a single pointing was made for each galaxy, using 1.5-3 arcsec/pixels, giving a total field of view for the  $32 \times 32$  pixel array of 0.8-1.6 arcmin. The spatial resolution is 4-8 arcsec limited by the full width at half maximum (FWHM) of the point spread function (PSF). High spatial resolution and sensitivity are essential in our analysis in order to isolate the central regions in nearby galaxies. Approximately 12 exposures of 2-5s each were made at each wavelength in addition to  $\sim 20$  exposures at the start of each observation to decrease the initial detector transient effects.

The raster maps were made with various broad band filters designed to select distinct features such as the continuum emission of the very small grains using the LW3(12-18  $\mu\text{m}$ ) filter, and the UIBs with the LW2(5-8.5  $\mu\text{m}$ ) and LW4(5.5-6.5  $\mu\text{m}$ ) filters. Depending on the apparent size of the galaxy, a pixel field of view of 1.5 or 3 arcsec was selected. Most of the maps were  $2 \times 2$  rasters with 6 pixel overlap consisting of approximately 200 exposures of 2-5s each. Another 30 exposures were added at the start of the observations to decrease the effects of transients.

The ISOCAM data were analyzed with the CAM Interactive Analysis software (CIA<sup>1</sup>) and were calibrated with the general methods described in Starck et al. (1999). To correct for the dark current, a dark model taking into account the observing time parameters was subtracted. Cosmic ray hits were removed by applying a multiresolution median filtering (Starck et al. 1996). Corrections of detector memory effects were made with the so-called inversion method (Abergel et al. 1996). The flat field correction was performed using the library of calibration data. Finally, individual exposures were combined using shift techniques

in order to correct the jitter effect due to the satellite motions (amplitude  $\sim 0.5$  arcsec). To derive the photometry of individual galaxy regions, aperture corrections as well as deconvolution techniques (Starck et al. 1998), were applied to account for the overall extension of the PSF in a few cases. We estimate that the absolute uncertainty of our photometric measurements is  $\sim 20\%$  while the error in the relative uncertainty mainly due to errors on transient effect correction is  $\sim 10\%$ .

## 3. MIR emission of normal, starburst galaxies and AGNs.

MIR spectra (5-16  $\mu\text{m}$ ) in galaxies can mainly arise from a variety of physical components including: 1) the evolved stellar population (Rayleigh-Jeans regime), which can dominate in early-type galaxies, 2) emission from the ionized interstellar gas, 3) non-thermal emission from radio sources and 4) dust particules responsible for the underlying continuum and 5) carriers of UIBs centered at 6.2, 7.7, 8.6, 11.3 and 12.7  $\mu\text{m}$ . The UIBs are thought to be due to C=C and C-H stretching and bending vibration modes in carbonaceous materials (Léger & Puget 1984, Allamandola et al. 1985, Papoular et al. 1989) and they dominate the MIR spectra of galaxies with low or intermediate star formation activity (Mattila et al. 1999) as in PDRs (Klein et al. 1999) and diffuse galactic regions (Giard et al. 1988, Mattila et al. 1996). The dust emitting longward of about 10  $\mu\text{m}$ , is attributed to Very Small Grains (here-after VSGs) with radius less than 10 nm (Désert et al. 1990), and is prominent in regions actively forming stars, such as Galactic HII regions (e.g. Verstraete et al. 1996, Cesarsky et al. 1996b) and in starburst regions. To emit in the MIR, the carriers of the UIBs and the VSGs are thought to be stochastically heated by the stellar radiation field reaching temperature fluctuations of the order of 100-1000 K (Puget & Léger 1989, Désert et al. 1990). The emission from ionized gas is mainly observed through forbidden lines such as [ArII](6.9  $\mu\text{m}$ ), [NeVI](7.6  $\mu\text{m}$ ), [ArIII](8.9  $\mu\text{m}$ ), [SIV](10.5  $\mu\text{m}$ ), [NeII](12.8  $\mu\text{m}$ ), [NeV](14.3  $\mu\text{m}$ ) and [NeIII](15.6  $\mu\text{m}$ ). Because of their high ionization potential, these lines can be used to trace the hardness of the radiation field. The presence of [NeVI] and [NeV] has also provided evidence for AGNs (Moorwood et al. 1996, Genzel et al. 1998, Sturm et al. 2000) or supernova remnants (Oliva et al. 1999).

In order to understand how the total MIR emission in our sample of starbursts and AGNs varies according to these different contributions, we first review the well-studied MIR properties in resolved nearby galaxies from early-type to later type disk galaxies and then address our observations in light of these properties.

<sup>1</sup> CIA is a joint development by the ESA astrophysics division and the ISOCAM consortium led by the ISOCAM PI, C. Cesarsky, Direction des Sciences de la matière, C.E.A. France.

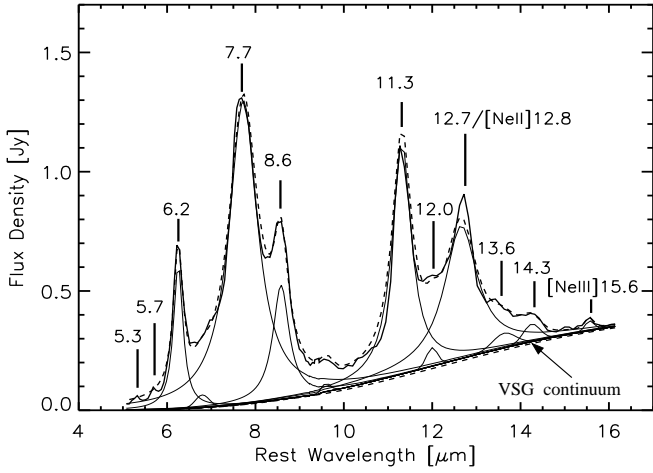


**Fig. 1.** Typical spectrum of a quiescent star forming region. The MIR spectrum (5-16  $\mu\text{m}$ ) of a disk region of M82 away from the central starburst (thick solid line), chosen for its high signal to noise ratio, is compared to a modeled spectrum (dashed line) including a continuum and UIBs. The dust continuum due to the VSGs is modeled by a black-body curve ( $T=200$  K) reddened by a dust absorption law with  $A_V=6$  mag (Dudley & Wynn-Williams 1997). The UIBs marked with the rest wavelength of their peak emission are modeled by lorentzian profiles (thin solid lines) (cf. Boulanger et al. 1998). Note the faint [NeIII] emission and the probable contamination of the [NeII]12.8  $\mu\text{m}$  line with the 12.7  $\mu\text{m}$  UIB feature. Faint UIBs are also detected at 5.3, 5.7, 12.0, 13.6, and 14.3  $\mu\text{m}$  as in many other galaxies of our sample.

### 3.1. MIR emission of “normal” galaxies: early to late type

The MIR spectra of elliptical galaxies, usually poor in cold gas and dust, are produced primarily by their evolved stellar population, and can be shown to resemble a black-body continuum with temperatures ranging from 4000 to 6000K (Madden et al. 1997, Boselli et al. 1998). This stellar emission accounts for most of the MIR emission of some elliptical galaxies. However, a non-negligible fraction of elliptical galaxies shows emission from UIBs and hot dust (Knapp et al. 1996a, Knapp et al. 1996b, Madden et al. 1999), as well as emission from non-thermal sources.

The MIR spectra of spiral galaxies, rich in gas and dust, are largely dominated by the UIBs. The observed UIB features show little spectral variations, and the total broad band LW3(12-18  $\mu\text{m}$ )/LW2(5-8.5  $\mu\text{m}$ ) flux ratio is close to 1 (Boselli et al. 1998, Roussel et al. 1999a, Roussel et al. 1999b). This ratio has been proposed as an indicator of the fraction of the VSG continuum to the UIB feature emission. As an example of the “typ-

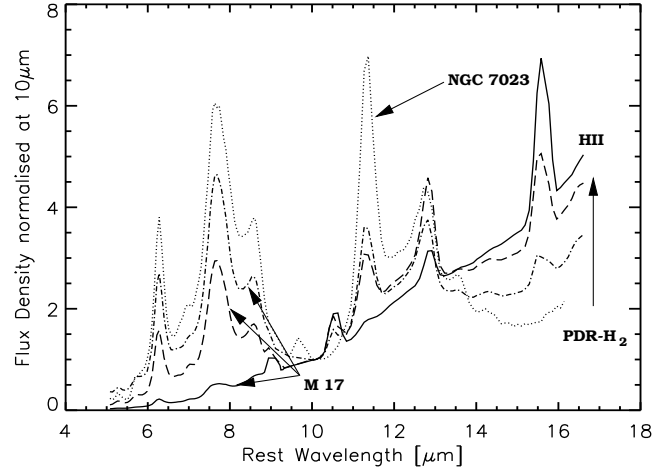


**Fig. 2.** MIR spectra showing the variation of the SED from a pure HII region, depicted by a solid line (close to OB stars in M17, Cesarsky et al. 1996b), to an isolated PDR indicated by a dotted line (NGC 7023, Cesarsky et al. 1996a). Each spectrum was normalized to the continuum at 10  $\mu\text{m}$ . The evolution is indicated by the vertical arrow which shows how the spectrum changes as we move from the outskirts of the HII region (dotted line) towards its core and near the OB stars (dashed and solid lines). Note how the strength of the UIBs progressively diminishes and how the continuum emission increases.

ical” integrated MIR emission of normal spiral galaxies, we present in Figure 1 the spectrum of a region in the disk of M82, 45 arcsec away from the central starburst. The usual UIB features, fitted by lorentzian profiles, are prominent. In addition, we notice the presence of several faint UIBs at 5.3, 5.7, 12.0, 13.6 and 14.3  $\mu\text{m}$  (Verstraete et al. 1996, Beintema et al. 1996, Sloan et al. 1999). Similar MIR spectra are also found in regions of the Galactic disk (Cesarsky et al. 1996a, Boulanger et al. 1996).

### 3.2. MIR emission of starburst galaxies.

The MIR spectra of galaxies with evidence of starburst activity have distinct features compared to normal spiral galaxies. Their most prominent characteristic is the presence of a very steeply rising continuum at 12-16  $\mu\text{m}$  from the VSGs. In starburst regions, this continuum is primarily produced in HII regions, tracing regions of massive star formation activity. The hard radiation field from young stars also excites ionic lines from [ArII], [ArIII], [SIV], [NeII] and [NeIII] which can be seen in the MIR spectra of starbursts. We display an example of this continuum in Figure 2 (solid line) using the spectrum near a pure HII region observed in M17, where the MIR emission is almost completely dominated by the VSG continuum (Cesarsky et al. 1996b). The weak intensity of UIBs

**Table 1.** Our galaxy sample

Source	RA (J2000)	DEC (J2000)	LW2 (mJy)	LW3 (mJy)	LW4 (mJy)	<u>LW3</u> LW2	<u>LW2</u> LW4	Spectral type LW	type CVF
NGC 1068(Nuc : 9") (2)	02 <sup>h</sup> 42 <sup>m</sup> 40.6 <sup>s</sup>	-00° 00' 47.8"	13009	46616	10221	3.58	1.27	AGN	AGN
Arp 118(Nuc : 3") (4)	02 <sup>h</sup> 55 <sup>m</sup> 12.2 <sup>s</sup>	-00° 11' 00.8"	16	42	10	2.62	1.62	AGN	AGN
NGC 3147(Nuc : 9") (5) <sup>†</sup>	10 <sup>h</sup> 16 <sup>m</sup> 53.6 <sup>s</sup>	73° 24' 03.3"	8	22	9	2.60	0.90	AGN <sup>+</sup>	-
Centaurus A(Nuc : 4.5") (6)	13 <sup>h</sup> 25 <sup>m</sup> 27.6 <sup>s</sup>	-43° 01' 08.8"	575	1658	500	2.89	1.15	AGN	AGN
NGC 6814(Nuc : 9") (7) <sup>†</sup>	19 <sup>h</sup> 42 <sup>m</sup> 40.6 <sup>s</sup>	-10° 19' 24.6"	33	85	31	2.59	1.05	AGN	-
NGC 253(Nuc : 7.5") (6)	00 <sup>h</sup> 47 <sup>m</sup> 33.1 <sup>s</sup>	-25° 17' 17.8"	4703	15716	2296	3.34	2.05	HII	HII
Arp 236(Nuc : 4.5") (3)	01 <sup>h</sup> 07 <sup>m</sup> 47.5 <sup>s</sup>	-17° 30' 25.6"	200	358	108	1.79	1.84	PDR	AGN*
NGC 1808(Nuc : 9") (1)	05 <sup>h</sup> 07 <sup>m</sup> 42.3 <sup>s</sup>	-37° 30' 46.1"	1074	1450	538	1.35	2.00	PDR	PDR
M82(Nuc : 9") (6)	09 <sup>h</sup> 55 <sup>m</sup> 52.2 <sup>s</sup>	69° 40' 46.9"	5198	12720	2573	2.45	2.02	HII	HII
NGC 3256(Nuc : 4.5") (1)	10 <sup>h</sup> 27 <sup>m</sup> 51.8 <sup>s</sup>	-43° 54' 08.7"	442	1196	212	2.70	2.09	HII	HII
Arp 299(A : 4.5") (1)	11 <sup>h</sup> 28 <sup>m</sup> 34.2 <sup>s</sup>	58° 33' 46.5"	325	1860	108	5.73	3.00	HII <sup>+</sup>	HII <sup>+</sup>
Arp 299(B : 4.5") (1)	11 <sup>h</sup> 28 <sup>m</sup> 31.5 <sup>s</sup>	58° 33' 40.4"	505	1951	303	3.86	1.67	HII	HII
Arp 299(C' : 4.5") (1)	11 <sup>h</sup> 28 <sup>m</sup> 31.8 <sup>s</sup>	58° 33' 49.9"	76	232	36	3.06	2.14	HII	HII
Arp 299(C : 4.5") (1)	11 <sup>h</sup> 28 <sup>m</sup> 31.2 <sup>s</sup>	58° 33' 48.9"	126	461	65	3.66	1.93	HII	HII
NGC 4038(KnotA : 6") (8)	12 <sup>h</sup> 01 <sup>m</sup> 54.9 <sup>s</sup>	-18° 53' 12.3"	23	135	13	5.78	1.75	HII	HII
Arp 220(9)	15 <sup>h</sup> 34 <sup>m</sup> 57.2 <sup>s</sup>	23° 30' 10.8"	162	732	79	4.50	2.07	HII	HII
NGC 6240(9)	16 <sup>h</sup> 52 <sup>m</sup> 58.5 <sup>s</sup>	02° 24' 03.4"	229	758	107	3.30	2.14	HII	HII
IRAS 17208-0014(1) <sup>†</sup>	17 <sup>h</sup> 23 <sup>m</sup> 21.9 <sup>s</sup>	-00° 17' 00.4"	127	248	60	1.96	2.11	PDR	-
IRAS 19254-7245(1) <sup>†</sup>	19 <sup>h</sup> 31 <sup>m</sup> 21.6 <sup>s</sup>	-72° 39' 20.2"	111	264	84	2.37	1.33	AGN*	-
IRAS 20551-4250(1) <sup>†</sup>	20 <sup>h</sup> 58 <sup>m</sup> 26.8 <sup>s</sup>	-42° 39' 00.6"	123	425	62	3.47	1.99	HII	-
IRAS 23128-5919(1)	23 <sup>h</sup> 15 <sup>m</sup> 47.0 <sup>s</sup>	-59° 03' 14.0"	90	319	53	3.54	1.70	HII	HII
NGC 253(Disk)(1)	00 <sup>h</sup> 47 <sup>m</sup> 33.1 <sup>s</sup>	-25° 17' 17.8"	339	681	171	2.00	1.98	PDR	PDR
NGC 520(1)	01 <sup>h</sup> 24 <sup>m</sup> 34.8 <sup>s</sup>	03° 47' 30.8"	486	511	231	1.05	2.10	PDR	PDR
NGC 1068(Disk)(2)	02 <sup>h</sup> 42 <sup>m</sup> 40.6 <sup>s</sup>	-00° 00' 47.8"	246	296	137	1.20	1.80	PDR	PDR
NGC 1808(Disk)(1)	05 <sup>h</sup> 07 <sup>m</sup> 42.3 <sup>s</sup>	-37° 30' 46.1"	1615	2694	728	1.67	2.22	PDR <sup>+</sup>	PDR
M 82(Disk)(1)	09 <sup>h</sup> 55 <sup>m</sup> 52.2 <sup>s</sup>	69° 40' 46.9"	1177	1133	589	0.96	2.00	PDR	PDR
NGC 3147(5) <sup>†</sup>	10 <sup>h</sup> 16 <sup>m</sup> 53.6 <sup>s</sup>	73° 24' 03.3"	375	483	215	1.29	1.74	PDR	-
NGC 3256(Disk)(1)	10 <sup>h</sup> 27 <sup>m</sup> 51.8 <sup>s</sup>	-43° 54' 08.7"	202	420	85	2.07	2.38	PDR <sup>+</sup>	PDR <sup>+</sup>
NGC 3263(Nuc : 4.5") (1) <sup>†</sup>	10 <sup>h</sup> 29 <sup>m</sup> 13.1 <sup>s</sup>	-44° 07' 22.0"	59	62	31	1.03	1.94	PDR	-
NGC 4676(A)(1) <sup>†</sup>	12 <sup>h</sup> 46 <sup>m</sup> 10.1 <sup>s</sup>	30° 43' 57.2"	58	30	40	0.53	1.44	PDR <sup>+</sup>	-
NGC 4676(B)(1) <sup>†</sup>	12 <sup>h</sup> 46 <sup>m</sup> 11.4 <sup>s</sup>	30° 43' 23.1"	4.11	2.15	2.17	0.52	1.89	PDR	-
Centaurus A(Disk)(10)	13 <sup>h</sup> 25 <sup>m</sup> 27.6 <sup>s</sup>	-43° 01' 08.8"	62	101	35	1.62	1.78	PDR	PDR
NGC 6814(6) <sup>†</sup>	19 <sup>h</sup> 42 <sup>m</sup> 40.6 <sup>s</sup>	-10° 19' 24.6"	291	290	144	1.00	2.02	PDR	-
NGC 7252(1)	22 <sup>h</sup> 20 <sup>m</sup> 44.9 <sup>s</sup>	-24° 40' 41.3"	142	185	67	1.30	2.11	PDR	-

**Table note:** Our galaxy sample is presented in three parts. The top includes nuclei of galaxies containing an AGN, the middle contains regions harboring starburst activity and the bottom presents quiescent star forming regions. The spectral type column indicates which of the three components (HII, PDR or AGN) provides the dominant contribution. Two values, one according to our broad band diagnostic (left column, see also Fig. 8) and one based on the CVF diagnostic (right column, see also Fig.6) are presented. The broad band fluxes for most galaxies have been calculated from their CVF spectra. NGC 7252 was observed in the CVF mode but due to its weak continuum emission the errors of the CVF diagnostic are large so we include only the LW classification. In NGC 4676(A), the MIR spectral energy distribution is probably contaminated by stellar emission (Hibbard & van Gorkom 1996, Read & Ponman 1998).

Notation used: “Nuc”= nucleus with the diameter in arcsec, “Disk”= well detected star formation region in the disk. References: <sup>1</sup> This work; <sup>2</sup> Laurent et al. 1999a; <sup>3</sup> Laurent et al. 1999c; <sup>4</sup> Charmandaris et al. 2000; <sup>5</sup> Laurent et al. 1997; <sup>6</sup> Laurent et al. 2000a; <sup>7</sup> Laurent et al. 1999b; <sup>8</sup> Mirabel et al. 1998; <sup>9</sup> Charmandaris et al. 1999; <sup>10</sup> Mirabel et al. 1999. The identification of specific regions in Arp 299, NGC 4038 and NGC 4676 follows the usual notation found in the literature. Galaxies marked with <sup>†</sup> have been observed only in broad band filter mode (LW). Galaxies marked with <sup>+</sup> identify those which clearly fall outside the limits of our diagnostic, as shown in Figure 6 and 8 and are classified to their nearest MIR spectral type. The galaxies marked by \* have not been previously classified as AGN-dominant, but have MIR characteristics which our diagnostics suggest as those of an AGN.

is interpreted as a consequence of the destruction of their carriers. However, since the UIBs originate from diffuse regions as well as PDRs surrounding HII regions, where they peak (Cesarsky et al. 1996a, Verstraete et al. 1996, Mattila et al. 1996, Tran 1998), strong UIBs can be detected in the MIR spectrum of embedded starburst regions. Consequently, this depletion of the UIB carriers will be further enhanced relative to the observed relative increase of the MIR continuum in starburst regions (see spectrum of Knot A in the Antennae Galaxies, Mirabel et al. 1998). Therefore, the LW3(12-18  $\mu\text{m}$ ) to LW2(5-8.5  $\mu\text{m}$ ) flux ratio increases in strong starburst environments. One should note that the overall MIR spectral shape can be also considerably affected by the high extinction often found in starburst regions. In particular the silicate band centered at 9.7  $\mu\text{m}$  can suppress the strength of UIBs at 11.3, 8.6 and 6.2  $\mu\text{m}$  relative to that at 7.7  $\mu\text{m}$  (Lutz et al. 1998, Rigopoulou et al. 1999) as seen in the spectrum of Arp 220 (Charmandaris et al. 1999).

### 3.3. MIR emission of AGNs.

Several studies have already shown that MIR spectra in AGNs also present weak UIBs (Roche et al. 1991, Genzel et al. 1998, Schulz et al. 1998, Rigopoulou et al. 1999, Dudley 1999). This effect is demonstrated in the spectrum of the nearest AGN of our sample located in the radio galaxy Centaurus A (CenA, NGC 5128, Mirabel et al. 1999).

In the MIR observations of CenA, we have sufficient spatial resolution to disentangle the emission of the central regions near the AGN from that due to star forming regions of the galactic disk. The absence of UIBs in the central 5 arcsec ( $\sim 100$  pc) possibly indicates the destruction of their carriers by the intense UV-X-ray radiation field from the AGN (Léger et al. 1989, Allain et al. 1996). Moreover, there is a noticeable continuum at short wavelengths (3-10  $\mu\text{m}$ ) commonly attributed to hot dust, associated with the torus of molecular gas proposed in the unified model (Pier & Krolik 1992, Granato et al. 1997, Murayama et al. 2000). The alternative interpretation of supernova remnants (SNRs) as the physical mechanism explaining the AGN phenomenon (Terlevich et al. 1992) is not supported by the MIR observations. Nearby SNRs, such as Cassiopeia A, Kepler, the Crab, RCW 103 and IC443 are all characterized by strong ionic and/or molecular line emission and a faint continuum (Douvion et al. 1999, Oliva et al. 1999). These characteristic features are not found in our integrated MIR spectra of galactic nuclei which are known to harbor AGNs. The MIR spectrum of AGNs is flatter compared to that of pure HII regions (see the AGN and HII spectra in Figure 5). This is in agreement with IRAS observations where infrared spectra from active galaxies are generally significantly flatter with the peak of emission shifted towards the MIR (de Grijs et al. 1985). Near an AGN the

radiation field can heat dust up to evaporation temperatures of  $\sim 1000\text{K}$  for silicate and  $\sim 1500\text{K}$  for graphite. As a result, the dust continuum emission becomes prominent at short wavelengths (3-6  $\mu\text{m}$ ) in contrast to emission from star forming regions which appears at longer wavelengths (e.g. Barvainis 1987). Such a continuum is found in the center of all galaxies in our sample known to be hosting an AGN such as NGC 1068, NGC 6814 or NGC 3147 (Laurent et al. 1997). Highly ionized species tracing the hard radiation field of the AGN (e.g. [NeV]14.3  $\mu\text{m}$  and [NeVI]7.6  $\mu\text{m}$ ) are detected in NGC 1068. However, due to the low spectral resolution of ISOCAM spectra ( $\lambda/\Delta\lambda \sim 40$ ), the [NeV] and [NeVI], if they exist, are blended with the nearby UIBs in all of our galaxies (see also Sturm et al. 2000).

## 4. MIR diagnostics to distinguish AGNs, starburst and quiescent star forming regions.

Our diagnostics are based on the assumption that the integrated MIR emission in galaxies can be represented by a sum of contributions originating from (1) regions where the dust is predominantly heated by an AGN and (2) regions where star formation is the main source of energy. As mentioned in sections 3.1 and 3.2, star forming regions can also be divided in two classes: relatively quiescent regions where most of the MIR emission originates from the PDRs, and starburst-like regions where continuum emission at 15  $\mu\text{m}$  produced in the HII regions is dominant. We therefore propose to categorize the spectra from our sample using empirical criteria chosen to separate the distinct UIB and MIR continuum behaviours. To further examine the relative proportion of each contribution, we also compare our spectra with three templates, namely, AGNs, pure HII regions and isolated PDRs. The relative proportions of these templates required to reproduce a given MIR spectrum allow us to classify the observed region as MIR spectral type dominated by AGN, starburst or relatively quiescent regions.

### 4.1. MIR templates

To construct the templates of each component, we selected three ISOCAM CVF spectra dominated by each of these physical processes. These template spectra are presented in Figure 5a.

The strong continuum at 14-15  $\mu\text{m}$  observed in starburst galaxies was modeled by a typical pure HII Galactic region spectrum from M17 (Cesarsky et al. 1996b). UIBs are absent or faint (upper panel of Figure 5a) and the [ArIII](8.9  $\mu\text{m}$ ), [SIV](10.5  $\mu\text{m}$ ), [NeII](12.8  $\mu\text{m}$ ) and [NeIII](15.6  $\mu\text{m}$ ) are present. A typical starburst spectrum can be usually decomposed using the VSG continuum with some UIB emission (Tran 1998). Since UIBs originate mainly from PDRs or diffuse regions, we used as their template, an isolated PDR spectrum from the galactic re-

flexion nebula NGC 7023 (Cesarsky et al. 1996a) (see the lower right part of the Figure 5a).

The AGN component was characterised by the MIR spectrum of the central region of CenA (see Fig. 3 and the lower left part of the Figure 5a), in which UIBs are absent as in the HII region template. However, in contrast to the HII region template spectrum, the continuum at short wavelengths (5-10  $\mu\text{m}$ ) is prominent in the AGN spectrum. In addition, the equivalent width of emission lines of [NeII] and [NeIII] is small, perhaps due to the overwhelming continuum contribution. Note that extinction affects the AGN template and is greater in Cen A than in NGC 1068 (see Fig. 10).

#### 4.2. MIR indicators: [HII]/[AGN] and [PDR]/[AGN,HII]

As each MIR template has distinct characteristics, we can quantify their relative contribution to the integrated spectrum. We have used two indicators based on the UIB strength and the MIR continuum. As an indicator of the relative HII region and AGN contribution, we use the ratio of “warm” (14-15  $\mu\text{m}$ ) to “hot” (5.1-6.8  $\mu\text{m}$ ) continuum (Fig. 4). As this ratio decreases, the presence of an AGN becomes more evident due to the increase of the relative importance of the “hot” continuum. The UIB(6.2  $\mu\text{m}$ ) to continuum (5.1-6.8  $\mu\text{m}$ ) flux ratio can be used to identify the relative contributions of the quiescent star forming regions to the starburst and/or AGN MIR emission. This indicator is very similar to the one proposed by Genzel which is based on the strength of the 7.7  $\mu\text{m}$  feature (Genzel et al. 1998, Lutz et al. 1998). Our estimate of the UIB flux has the advantage to be less affected by the strong silicate extinction at 9-11  $\mu\text{m}$  while the continuum at 5-7  $\mu\text{m}$  is also less contaminated by the VSG continuum. The effect of a strong absorption on the AGN continuum could artificially enhance the presence of a UIB at 7.7  $\mu\text{m}$  but not at 6.2  $\mu\text{m}$ . Nevertheless, the choice of the 6.2  $\mu\text{m}$  which is weaker than the 7.7  $\mu\text{m}$  feature necessitates spectra with good signal to noise ratio. This is the case in our sample of spectra where the UIB at 6.2  $\mu\text{m}$  is very well detected (Figures 3 and 7 or the spectra in the Antennae in Mirabel et al. 1998, for some examples). Since our primary goal is to establish the absence of UIBs as well as the presence of a well detected AGN continuum, at short MIR wavelengths, a criterion based on the UIB(5.9-6.8  $\mu\text{m}$ )/Continuum(5.1-6.8  $\mu\text{m}$ ) ratio applied on high signal to noise spectra gives a more accurate diagnostic for revealing the presence of an AGN. As we show in the following sections, the relative variation of our UIB/Continuum at 6  $\mu\text{m}$  is reliable in separating a featureless continuum from UIB spectra even if our 6  $\mu\text{m}$  continuum measurements may still be slightly affected by emission coming from the wing of the 7.7  $\mu\text{m}$  UIB (see Fig. 4).

#### 4.3. Diagnostic diagram

Having defined the three MIR templates, we construct a complete library of composite spectra where the contribution of each template can vary between 0 and 100 %. On these composite spectra, we can measure the diagnostic ratios presented above and plot them on a 2-dimensional diagram (see Fig. 5). Three main regions can be identified in the corners of this diagram where the signatures of AGNs, starbursts, or quiescent star forming regions dominate the total spectrum.

The above diagram can be applied only in the galaxies where MIR spectra are available. However, one may expand it to cases where only broad band MIR images are available. This can be done by using our library of spectra to estimate their corresponding fluxes through the ISOCAM filters that isolate as closely as possible the regions identified in Figure 4. The filters used are the LW2(5-8.5  $\mu\text{m}$ ), LW3(12-18  $\mu\text{m}$ ) and LW4(5.5-6.5  $\mu\text{m}$ ). As we will show in the following sections the broad band diagnostic gives results comparable to those obtained with the CVFs. The equivalent fluxes of our CVF templates through the three broad band filters are presented in Figure 5b. Using the same reasoning as in Figure 5a, we estimate the relative strength of UIBs with the LW2(5-8.5  $\mu\text{m}$ )/LW4(5.5-6.5  $\mu\text{m}$ ) flux ratio while the ratio of the LW3(12-18  $\mu\text{m}$ )/LW2(5-8.5  $\mu\text{m}$ ) emission provides an estimate of the VSG contribution relative to the UIB and/or hot dust emission at short wavelengths. Those two diagnostic diagrams have in common the capacity to separate individually regions dominated by AGN, starburst or quiescent star forming regions. The robustness of the two criteria against observed MIR spectra of galaxies is examined in the following section.

#### 4.4. Application of the diagnostic

Our MIR indicators were applied to the galaxies of our sample (see Table 1), in which we also included a few irregular galaxies such as the blue compact dwarf galaxies IIZw40 and NGC 1569 (Madden et al. 1999) and barred spiral galaxies NGC 1097 and NGC 1365 (Roussel et al. 1999a) in order to cover the diagram completely. In cases where we had adequate spatial resolution, we extracted different physical regions in the same galaxy. The results are presented in Figure 6. Galaxies commonly classified as starbursts, such as Arp 220 and Arp 299(A), fall toward the top part of the diagram implying the presence of a large fraction of starburst regions compared to quiescent star forming regions. A few nearby galaxies with known AGNs are located in the bottom left part of the diagram along with our AGN template, the nucleus of Cen A. Regions of moderate star formation observed in galactic disks are situated in the region of the diagram where we expect to find a dominant PDR contribution. In Figure 7, we present three typical spectra from

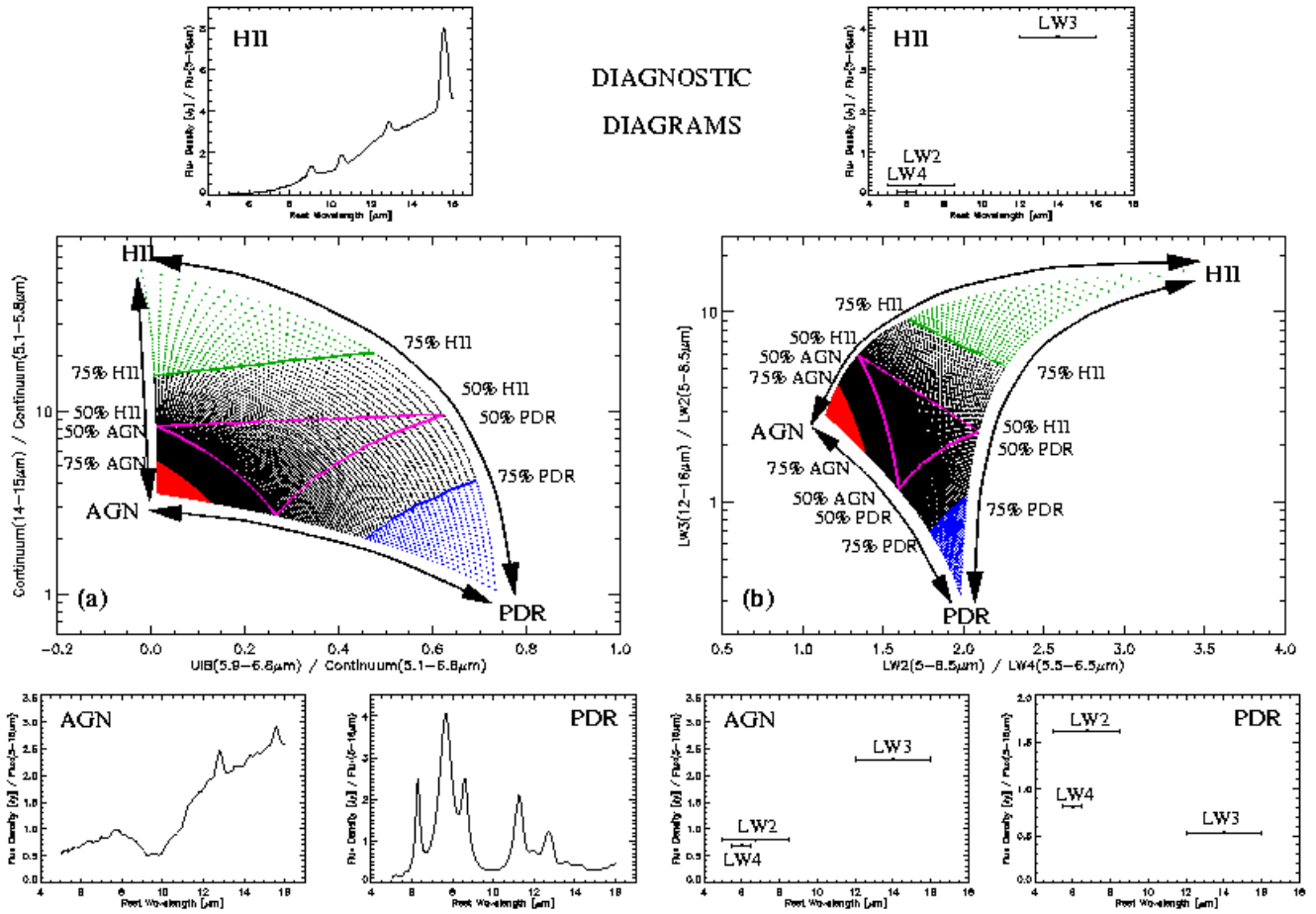


**Fig. 5.** a) Diagnostic diagram based on CVF spectra. b) Diagnostic diagram based on broad band filters. Three distinct areas can be defined. In the upper corner, we select spectra dominated by massive HII regions such as those found in starbursts. On the lower left, AGN spectra are dominant in a very small region, and finally, PDR spectra fall in the lower right part. The solid lines and the associated percentages indicate a constant fraction of one component along each line (see section 4.3).

our sample dominated by UIBs (the disk of M82), an HII continuum (the nucleus of M82) as well as an AGN (the nucleus of NGC 1068). Based on their position on our diagnostic diagram in Figure 6, we estimate the corresponding fraction of MIR templates according to the Figure 5a. This is a first order approximation since we do not take explicitly into account the effects of the  $9.7 \mu\text{m}$  silicate absorption band on our template spectra. Consequently, the observed difference between model and spectra in the range of  $9$  to  $11 \mu\text{m}$  is probably due to the strong silicate extinction in embedded starbursts or AGNs. We do not attempt to model the emission from the  $[\text{NeII}](12.8 \mu\text{m})$  and  $[\text{NeIII}](15.6 \mu\text{m})$  lines which are independent of the dust emission properties. Nevertheless, the overall agreement presented in Figure 7 is sufficient for modeling the general shape of spectra.

To extend our diagnostics in the case where spectra are not available, we present in Figure 8 the diagnos-

tic diagram using broad band filters<sup>2</sup>. As expected, the AGN candidates appear in the left part of this diagram. For LW3/LW2 ratios close to 1, PDRs dominate the MIR emission in our sample as it was the case for normal spiral galaxies (Boselli et al. 1997, Roussel et al. 1999a). For LW3/LW2 ratios between 1 and 6, both an AGN and a star forming region signature may appear in our spectra (e.g. the nucleus of NGC 253 and NGC 1068 in Fig. 8).

We note, however, that the LW2/LW4 flux ratio is well adapted to estimate the presence of an AGN contribution. For LW2/LW4 ratios lower than 1.5, we clearly see that the MIR emission is dominated by the AGN whose strong continuum and nearly absent UIBs, contribute to

<sup>2</sup> For galaxies of our sample for which we had only CVF spectra, we calculated the equivalent broad band filter fluxes taking into account their filter transmission. Note that since the CVF ends at  $16 \mu\text{m}$  to match its equivalent LW3 filter to the ISOCAM standard LW3( $12-18 \mu\text{m}$ ) filter, we have normalized the transmission of the latter between  $12$  and  $16 \mu\text{m}$ .

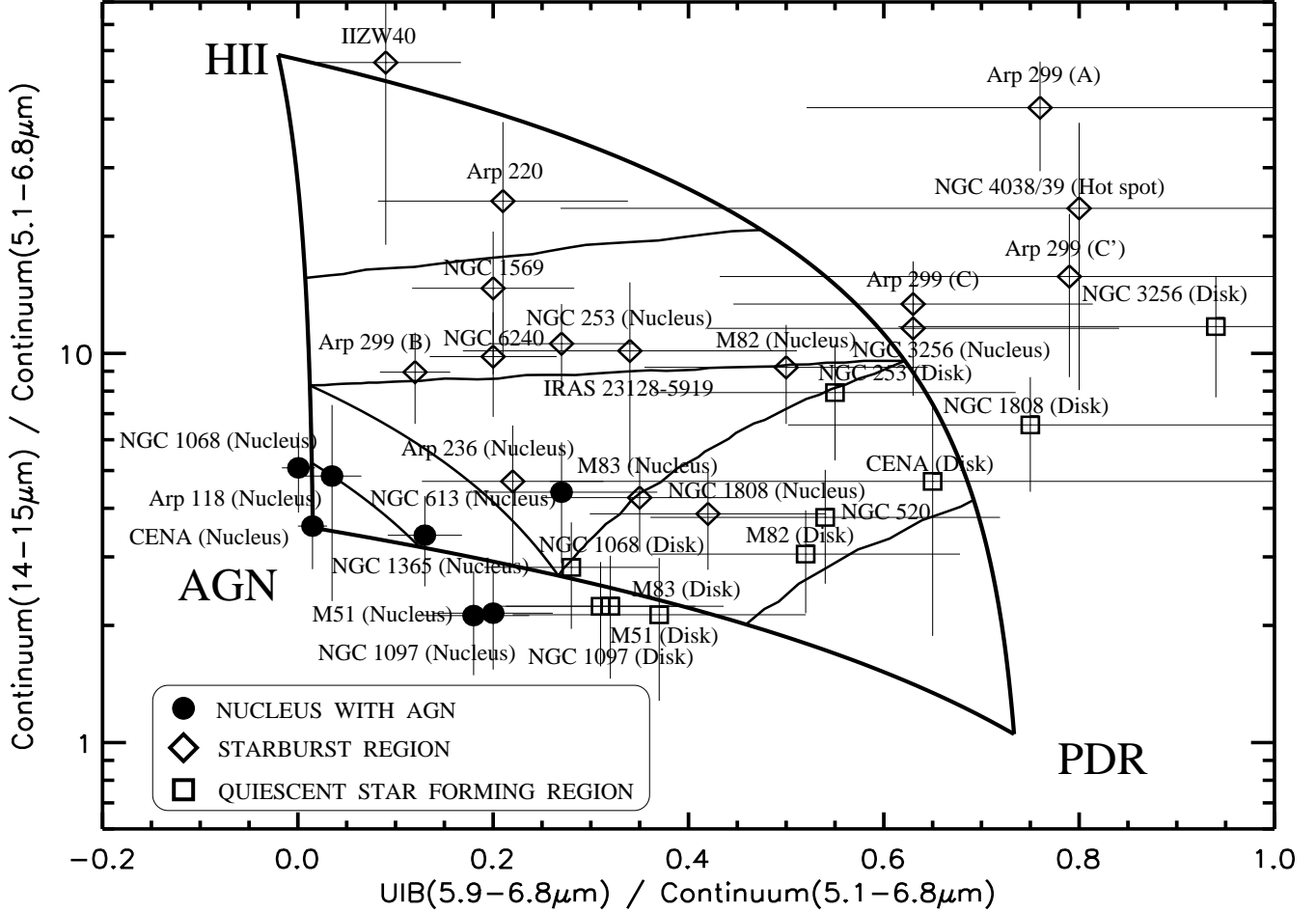


**Fig. 6.** Diagram based on CVF diagnostics for 33 spectra using the notation of Table 1. The error bars are estimated from the rms maps at  $1\sigma$  for each wavelength along the CVF spectra, added to a systematic error of 10% due to the transient correction method. Note that several spiral and blue compact dwarf galaxies included in this figure are not listed in the Table 1 since they belong to other samples (Madden et al. 1999, Roussel et al. 1999a). The circles mainly located in the bottom left part of the diagram represent the central regions known to contain an AGN. The galaxies hosting starburst activity are in the upper part and are marked with diamonds. The spectra of quiescent star forming regions are found to lie close to the PDR region and are denoted with squares. The curves demarcate the AGN, PDR and HII spectral type according to Figure 5a.

decrease this ratio. For larger LW2/LW4 ratios, emission is dominated either by quiescent star forming regions or by starburst regions (see Fig. 8). Applying this criterion to the nucleus of M82, we clearly see that it is classified as a starburst while the nucleus of NGC 1068 has a typical AGN signature. Although this diagram uses only three broad band filters, the MIR classification is in good agreement with results given by the diagnostic diagram based on full spectra (see Table 1).

Moreover, the diagnostic diagrams of Figures 6 and 8 suggest that the well-known ultra-luminous galaxies such as IRAS 23128-5919 and NGC 6240 have MIR spectra which are overwhelmed by a strong starburst signature. In the “Super Antennae” (IRAS 19254-7245), which

harbors a Seyfert 2 nucleus (Mirabel et al. 1991), more than  $\sim 70\%$  of its MIR flux originates from the AGN (Laurent et al. 2000b).

One can also use this technique to discover up to now unclassified AGN hidden by a large column density of dust. Such a candidate is Arp 236 (IC 1623, VV 114), an infrared luminous system ( $L_{IR} = 10^{11.62} L_{\odot}$ ), classified as an early-stage gas-rich merger ( $M(H_2) = 5.1 \times 10^{10} M_{\odot}$ , Yun et al. 1994), and composed of several nuclei and/or compact starburst regions. Previous near-infrared and radio studies showed no evidence for an AGN (Knop et al. 1994, Doyon et al. 1995). However, the MIR signatures of the eastern region (knot A, Doyon et al. 1995) place it near the AGN locus in our



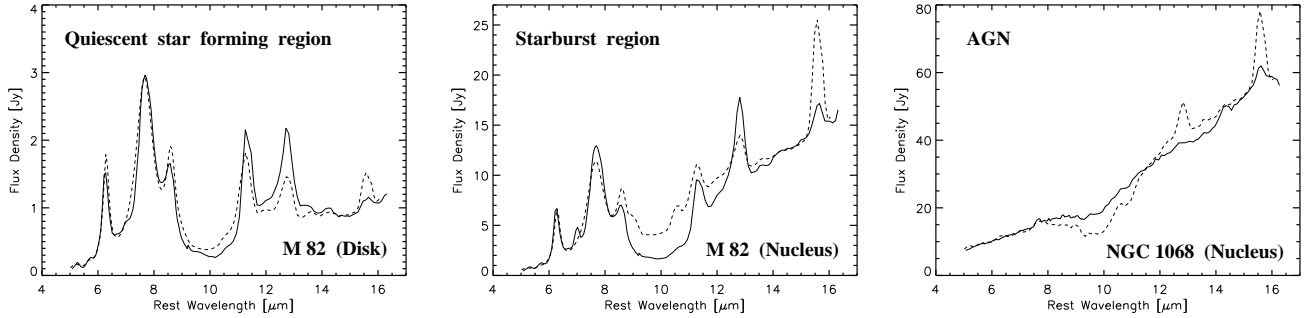


**Fig. 7.** Examples of spectra (solid lines) classified as dominated by star forming regions (the disk and the nucleus of M82) and by an AGN (the nucleus of NGC 1068) are shown with their corresponding model based on a combination of templates (dashed line). For each spectrum, we find the appropriate combination of templates (8%AGN, 50%HII, 42%PDR for the nucleus of M82; 8%AGN, 15%HII, 77%PDR for the disk of M82 and 77%AGN, 23%HII, 0%PDR for the nucleus of NGC 1068) using the location of those sources in the CVF diagram (see Fig. 6). Each composite spectrum has been normalised at 14-15  $\mu\text{m}$ .

CVF diagram (Fig. 6) and, therefore, may contain a non-negligible fraction of AGN contribution in its MIR spectrum. Nevertheless, one should note that the possible AGN contribution in Arp 236 is not revealed with the LW diagnostic (Fig. 8) which is less accurate compared to the CVF diagnostic. Knot A is the brightest source in the near-infrared. It is also redder and more compact than all other sources in the system (not resolved at 3.7  $\mu\text{m}$  with a FWHM of 0.3 arcsec, Knop et al. 1994). We estimate that  $\sim 40\%$  of the MIR emission in the region can originate from an optically obscured AGN. A MIR spectral classification based on our method is presented in the last column of Table 1 for all of our sample.

## 5. Discussion

Our diagnostic diagrams provide a new tool allowing us to identify an AGN or star formation (starburst and/or quiescent star forming regions) signature in the integrated MIR spectrum of a galaxy.

Although self consistent, our method is based on data from a rather diverse sample. To further test its validity, we compared it with the MIR diagnostics developed by Genzel et al. (1998a) on a complete sample of ULIRGs, using ISOPHOT-S. Using the published MIR spectra of the brightest sources in the Genzel sample, we calculated the strength of the UIB at 6.2  $\mu\text{m}$  in these spectra, as well as the equivalent LW2(5-8.5  $\mu\text{m}$ )/LW4(5.5-6.5  $\mu\text{m}$ ) ratio since this is the principal discriminator between an AGN and star forming regions (see Fig. 9). The classification of galaxies obtained based on our method is in complete agreement with that of Genzel et al. (1998a). IRAS 23060+0505, IRAS 19254-7245, Mrk 231 and Mrk 273, with an LW2/LW4 ratio of 1.16, 1.36, 1.42 and 1.60 respectively, are classified by both methods as galaxies containing a significant AGN contribution in the MIR. Furthermore, in the wavelength range of ISOCAM (5-16  $\mu\text{m}$ ), we can better constrain the nature of the continuum at

7  $\mu\text{m}$  between dust and stellar contribution using the 14-15  $\mu\text{m}$  flux, since the LW3(12-18  $\mu\text{m}$ )/LW2(5-8.5  $\mu\text{m}$ ) flux ratio is greater than 3 for the dust continuum found in AGNs or HII regions and less than 0.4 for the stellar continuum (Boselli et al. (1997)). We are also able to distinguish whether a featureless continuum is due to an AGN or a pure HII region (e.g. IIZw40).

Selective absorption by amorphous silicates, centered at 9.7 and 18  $\mu\text{m}$ , can play a crucial role in obscuring emission over much of the MIR wavelengths. AGNs embedded in a large amount of dust could still remain undetected by our diagnostic. Studying a sample of 28 Seyfert 1 and 29 Seyfert 2 with ISOPHOT-S, Schulz et al. (1998) have already shown that the high absorption in Seyfert 2 galaxies blocks a large fraction (90% on the average) of the MIR continuum from the AGN inner torus. They do detect the silicate feature in emission at 9.7  $\mu\text{m}$  which is in favour of a moderately thick torus model ( $A_V \sim 100$ , Granato et al. 1997) and rules out models with very large optical depths ( $A_V \sim 1000$ , Pier & Krolik 1992). In our sample, among all nuclei (diameter  $< 9''$ ) which are classified as AGNs based on our MIR diagnostics (see Fig. 8), five nuclei are optically selected as Seyfert 2. Provided sufficient spatial resolution is available, we can detect the hot dust continuum associated with the AGN and we are able to disentangle its contribution to the MIR emission of the galaxy. If those nuclei were observed with the ISOPHOT-S aperture of  $24 \times 24 \text{ arcsec}^2$ , we would detect the presence of an AGN only in the two nearest Seyfert 2 of our sample NGC 1068, CenA and in NGC 6814 which is a Seyfert 1. The dilution effect combined with the optical depth of the AGN torus would lead to an underestimation of the number of detected AGNs. The MIR continuum associated with AGNs is not completely suppressed behind the dusty torus and may be observed using sufficient spatial resolution ( $\sim 5 \text{ arcsec}$ ) observations on nearby galaxies ( $D < 50 \text{ Mpc}$

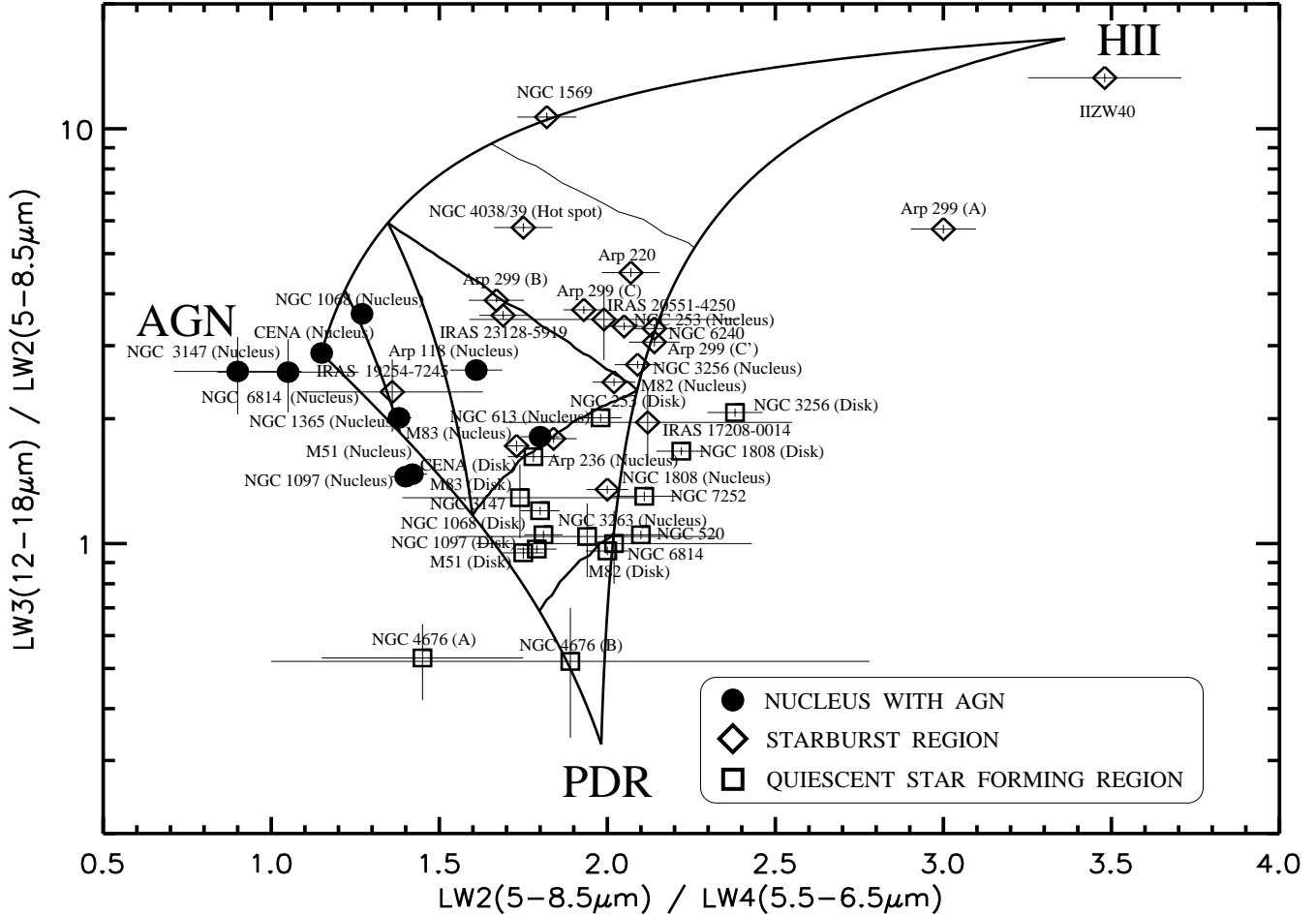


**Fig. 8.** Diagram based on broad band diagnostics for 45 spectra using the notation of Table 1. The error bars are estimated from the rms map at  $1\sigma$  for CVF spectra or broad band observations added to a systematic error of 10% due to the transient correction method. Note that several spiral and blue compact dwarf galaxies not listed in the Table 1 are from other samples (Roussel et al. 1999a, Madden et al. 1999). The galactic central regions (size of several kpc) hosting an AGN are all located in the left part of the diagram (marked with circles). The galaxies dominated by a starburst activity are in the upper part due to their higher LW3/LW2 ratio (marked with diamonds). The spectra of quiescent star forming regions lie close to the PDR area (marked with squares). The curves demarcate the AGN, PDR and HII spectral type according to Figure 5b.

with  $H_0=75 \text{ km s}^{-1} \text{ Mpc}^{-1}$ , see Laurent et al. 1999b). The detection of the AGN continuum in Seyfert 2 is also in better agreement with a dusty torus model producing moderate absorption ( $A_V \sim 100$ ) as in the model of Granato et al. (1997).

In Figure 10, we note that the increase of the absorption in an AGN spectrum leads to a decrease of the hot continuum used in our diagnostic. This further suggests that the “true” AGN fraction would be underestimated and our detections must be considered as a lower limit. An intrinsically low AGN contribution to the MIR spectrum of a source would be difficult to distinguish from the star forming emission at  $6\text{--}7 \mu\text{m}$  composed by UIBs and the VSG continuum. Consequently, we consider that an

AGN is detected by our diagnostic when the estimated fraction of the AGN emission is larger than the contribution of starburst or quiescent star forming regions.

Recently several studies on the origin of the MIR emission in galaxy clusters and deep field surveys were performed with ISOCAM using the LW3 and LW2 broad band filters (e.g. Aussel et al. 1999, Désert et al. 1999, Flores et al. 1999). Our diagnostic implies that one cannot discriminate between an AGN and a starburst signature using just those two filters in the local universe (see Fig. 9). At high redshifts, the two filter bandpasses sample shorter rest frame wavelength emission and are less sensitive to the VSG continuum. In Figure 11, we applied a redshift correction on our MIR templates at  $z=0.2$  and  $z=0.4$ , and

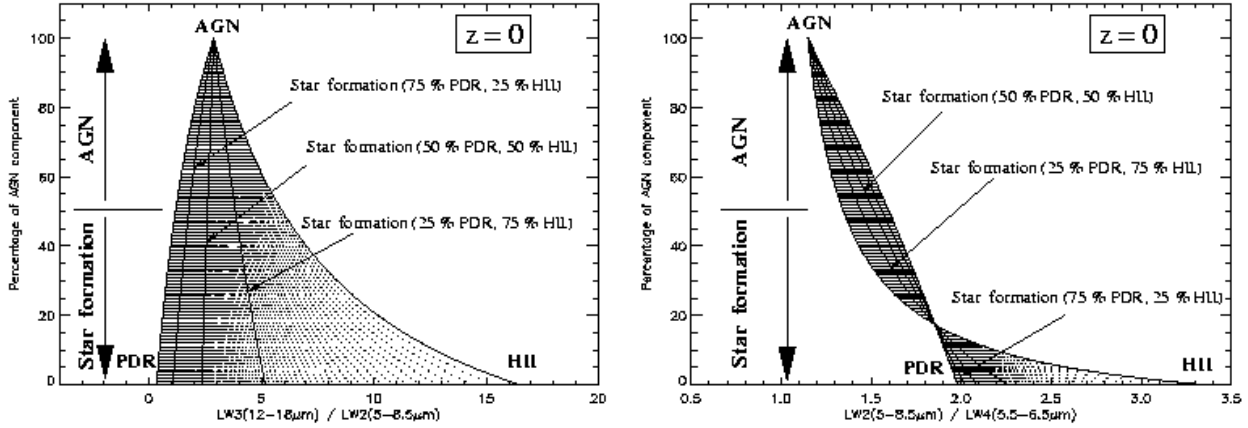


**Fig. 9.** a) In the above figure we display the variation of the AGN-Starburst fraction (indicated in the y-axis) as a function of  $LW3(12-18\ \mu\text{m})/LW2(5-8.5\ \mu\text{m})$  flux ratio based on the three templates of our diagnostic for galaxies of the local universe. We divide our library of composite spectra (see Fig. 5) into one component attributed to star formation activity (including both the PDR/diffuse and HII region templates) and a second one to AGN. For a given  $LW3/LW2$  ratio and a selected type of star formation mixture (as indicated by the solid curves of different PDR and HII fractions) one can calculate the percentage of the AGN component in the spectrum. b) Same as in a) but for the  $LW2(5-8.5\ \mu\text{m})/LW4(5.5-6.5\ \mu\text{m})$  flux ratio. Note how the use of just the  $LW3/LW2$  ratio is insufficient for detecting AGNs. This is not the case for the  $LW2/LW4$  ratio which is relevant to select AGNs from starbursts (see section 4.4).

we obtained the equivalent diagnostic diagrams derived from observations of nearby galaxies. To extrapolate the part of the spectrum under  $5\ \mu\text{m}$ , we use a power law for the AGN template and a black-body continuum for the pure HII region template. We also assume that the PDR component under  $5\ \mu\text{m}$  is negligible (Lu et al. 1999). At  $z=0.4$ , objects with  $LW3/LW2 < 3$  are classified as AGN-dominant in the MIR. For redshifts between 0.5 and 1, the  $LW3$  filter samples mainly UIBs ( $LW2$  at  $z=0$ ), while  $LW2$  probes the hot dust emission between 3 and  $5\ \mu\text{m}$  (assuming that the stellar emission is negligible in spiral galaxies and only begins to be substantial below  $2\ \mu\text{m}$ ). Consequently, low values of the  $LW3/LW2$  flux ratios in these surveys would suggest the presence of an AGN.

In our diagnostic method, we have implicitly considered that the MIR emission from the evolved stellar population is negligible in spiral galaxies. Even though this may be true for galactic disks (Roussel et al. 1999a), extra caution is needed for bulges in the center of which one finds the AGN. In that case, it is the rising slope of the MIR spectrum which would reveal the presence of an AGN, even though we cannot rule out completely a possible faint contamination from evolved starlight at short wavelengths. Moreover, the fact that the core radius of the bulge is several orders of magnitude larger than the region responsible for the “hot continuum” would in principle facilitate their separation in nearby galaxies. For distant galaxies where the integrated MIR spectra include the whole galactic bulge, it is very difficult to estimate the

form of the continuum below  $6\ \mu\text{m}$ . M83, a well known starburst galaxy, is such an example, since we detect considerable continuum emission at  $5-6\ \mu\text{m}$  (see Fig. 8). This emission is clearly extended outside the unresolved nuclear region and can be interpreted as stellar emission from the stellar bar (cf. Elmegreen et al. 1998 and Sauvage priv. comm.)<sup>3</sup>. Furthermore, for distant galaxies the contribution of the star forming regions surrounding an AGN would progressively enter in the beam and dilute the AGN MIR signatures. A more detailed discussion on this issue is presented in Laurent et al. 1999b.

Our diagnostic method can be further expanded with the improved performance of upcoming telescopes, and can be used as a guide in scheduling future research programs. In addition to an increase in sensitivity, SIRTf will provide better wavelength coverage ( $5-40\ \mu\text{m}$ ) than ISO-CAM, and better spatial resolution than the ISO-SWS observations. In particular, SIRTf would provide a better measurement of the continuum for distant faint sources and, calculating the depth of both silicate absorption bands at  $9.7$  and  $18\ \mu\text{m}$ , a more precise estimate for the absorption. An increase in spatial resolution would also permit a significant improvement in the AGN/Starburst diag-

<sup>3</sup> To further develop our diagnostic for general cases including evolved stellar population, the K band flux at  $2.2\ \mu\text{m}$  could be used to estimate the contribution of the stellar emission observed at short MIR wavelengths. A  $LW2/K$  or  $LW3/K$  flux ratio less than 1 would indicate a more important contribution from the stellar component.

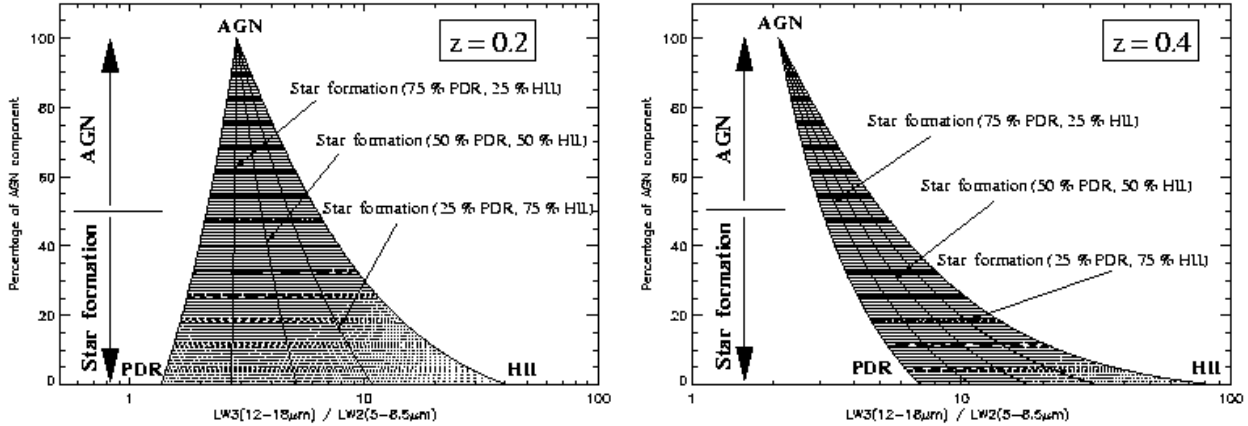


**Fig. 11.** Variation of the AGN-Starburst fraction at different redshifts ( $z=0.2$  on the left and  $z=0.4$  on the right) as a function of  $LW3(12-18\ \mu\text{m})/LW2(5-8.5\ \mu\text{m})$ . We use the same notation as in Figure 9 for the contribution of the star formation component. The percentages indicate the fraction of each contribution in the rest-frame wavelengths. The  $LW3/LW2$  ratio which is degenerate for distinguishing AGNs from starbursts at low redshifts can be used for detecting the AGN continuum at higher redshifts (i.e.  $z\sim 0.4$ ) due to the K-correction effect on MIR spectra (see section 5).

nostics. Both the infrared instruments installed on ground based 10 meter telescopes and the Next Generation Space Telescope which will cover the MIR spectrum, will probe regions of  $\sim 10$  pcs near the AGNs, decreasing significantly the effects of beam dilution.

## 6. Conclusions

Using our ISOCAM MIR observations we have obtained a new AGN/Starburst diagnostic based on the strength of the UIBs at  $6.2\ \mu\text{m}$  and the MIR continuum. We conclude that:

1) In AGN spectra (even with a faint starburst contamination), a strong MIR continuum is present at short wavelengths between  $3-10\ \mu\text{m}$ . This continuum may be attributed to very hot dust grains directly heated by the central engine. Furthermore, the absence of UIBs suggests that their carriers can be destroyed by the strong UV-X ray radiation field.

2) Our MIR diagnostic diagrams can be used to unravel AGNs that are completely obscured at optical wavelengths. For example, the nucleus of Arp 236 which was classified as a starburst galaxy triggered by an interaction is likely to contain an AGN that contributes  $\sim 40\%$  to the MIR flux.

3) The emission from ultraluminous infrared galaxies can be dominated either by a starburst (e.g. Arp 220) or an AGN (e.g. The Super Antennae, IRAS 19254-7245). Nevertheless, an AGN can remain partially hidden by the torus absorption even in the MIR which may lead to an underestimate of its contribution to the whole spectral energy distribution.

4) In the local universe, the  $LW3(12-18\ \mu\text{m})/LW2(5-8.5\ \mu\text{m})$  ratio alone cannot be used to distinguish AGNs from starbursts. However, for galaxies at  $z=0.4-1$ , this ratio is effective in discriminating the AGN from the starburst contribution.

5) Applications of adapted versions of our diagnostic in future instruments such as SIRTf and NGST, which will sample the MIR band with higher spatial resolution and sensitivity than ISOCAM, should provide better insights into the heating sources of the interstellar medium in galaxies.

*Acknowledgements.* We thank H. Roussel, D. Tran and T. Douvion for providing data in advance of publication as well as P.-A. Duc and D.B. Sanders for their help on various aspects of this work. We are grateful to C. Dudley for sending us his extinction curve. We thank the referee, C. Lonsdale, for useful suggestions which led to considerable improvement of this paper. VC would like to acknowledge the financial support from a Marie Curie fellowship (TMR grant ERBFMBICT960967).

## References

- Abergel A., Bernard J.P., Boulanger F., et al., 1996, A&A 315, L329
- Allamandola L.J., Tielens A.G.G.M., Barker J.R., 1985, ApJ 290, L25
- Allain T., Leach S., Sedlmayr E., 1996, A&A 305, 602
- Aussel H., Cesarsky C.J., Elbaz D., Starck J.L., 1998, A&A 342, 313
- Barvainis R. 1987, ApJ 320, 537
- Beintema D.A., van den Ancker M.E., Molster F.J. 1996, A&A 315, L369
- Boselli A., Lequeux J., Contursi A., et al., 1997, A&A 324, L13
- Boselli A., Lequeux J., Sauvage M., et al., 1998, A&A 335, 53

- Boulanger F., Boissel P., Cesarsky D., Ryter C., 1998, *A&A* 339, 194
- Boulanger F., Reach W.T., Abergel A., et al., 1996, *A&A* 315, L329
- Cesarsky C., Abergel A., Agnese P., et al., 1996, *A&A* 315, L32
- Cesarsky D., Lequeux J., Abergel A., et al., 1996a, *A&A* 315, L305
- Cesarsky D., Lequeux J., Abergel A., et al., 1996b, *A&A* 315, L309
- Charmandaris V., Laurent O., Mirabel I.F., et al., 1999, in *Ultraluminous Galaxies: Monsters or Babies?*, Ap&SS, Vol. 266, Issue 1-2, p. 99
- Charmandaris V., Laurent O., Mirabel I.F., et al., 2000, in *The Evolution of Galaxies on Cosmological Timescales*, Tenerife, Spain 1999, Ap&SS, (in press)
- Condon J.J., Huang Z.-P., Yin Q.F., Thuan T.X., 1991, *ApJ* 378, 65
- Désert F.-X., Boulanger F., Puget J.L., 1990, *A&A* 237, 215
- Désert F.-X., Puget J.-L., Clements D.L., et al., 1999, *A&A* 342, 363
- Douvion T., Lagage P.O., Ballet J., et al., 1998, in *ISO Conference: The Universe as seen by ISO*, p. 301
- Doyon R., Nadeau D., Joseph R.D., et al., 1995, *ApJ* 450, 111
- Dudley C.C., Wynn-Williams C.G., 1997, *ApJ* 488, 720
- Dudley C.C., 1999, *MNRAS* 307, 553
- Elmegreen D.M., Chromey F.R., Warren A.R., 1998, *AJ* 116, 2834
- Flores H., Hammer F., Désert F.X. et al., 1999, *A&A* 343, 389
- Gallais P., Laurent O., Charmandaris V. et al., 1998, *ISO Conference: The Universe as seen by ISO*, p. 880
- Genzel R., Lutz D., Sturm E., et al., 1998, *ApJ* 498, 579
- Giard M., Serra G., Caux E., Pajot F., Lamarre J.M., 1988, *A&A* 201, L1
- Goldader J.D., Joseph R.D., Doyon R., Sanders D.B., 1995, *ApJ* 444, 97
- Granato G.L., Danese L., Franceschini A., 1997, *ApJ* 486, 147
- de Grijp M.H.K., Miley G.K., Lub J., de Jong T., 1985, *Nature* 314, 240
- Hibbard J.E., van Gorkom J.H., 1996, *AJ* 111, 655
- Kessler M.F., Steinz J.A., Anderegg M.E. et al., 1996, *A&A* 315, L27
- Kim D.-C., Veilleux S., Sanders D.B., 1998, *ApJ* 508, 627
- Klein R., Henning T., Cesarsky D., 1999, *A&A* 343, L53
- Knapp G.R., Rupen M.P., 1996a, *ApJ* 460, 271
- Knapp G.R., Rupen M.P., Fich M., et al., 1996b, *A&A* 315, L75
- Knop R.A., Soifer B.T., Graham J.R., et al., 1994, *AJ* 107, 920
- Laurent O., Mirabel I.F., Charmandaris V., et al., 1997, in *XVIIth Moriond Astrophysics Meeting: Extragalactic Astronomy in the Infrared*, p. 311
- Laurent O., Mirabel I.F., Charmandaris V., et al., 1999a, in *The Evolution of Galaxies on Cosmological Timescales*, Tenerife, Spain 1999, Ap&SS, Vol. 266 (in press)
- Laurent O., Mirabel I.F., Charmandaris V., et al., 1999b, in *XIXth Moriond Astrophysics Meeting: Building the Galaxies: From the Primordial Universe to the Present*, p. 79
- Laurent O., Mirabel I.F., Charmandaris V., et al., 1999c, in *The Universe as Seen by ISO*, ESA SP-427, March 1999, p. 913
- Laurent O., Mirabel I.F., Charmandaris V., et al., 2000a, in *Toward a New Millennium in Galaxy Morphology*, Johannesburg, South Africa, p. 377 (in press)
- Laurent O., Mirabel I.F., Charmandaris V., et al., 2000b, *A&A* in preparation
- Léger A., Puget J.L., 1984, *A&A* 137, L5
- Léger A., D'Hendecourt L., Boissel P., et al., 1989, *A&A* 213, 351
- Lonsdale C.J., Smith H., Lonsdale C.J., 1993, *ApJ* 405, L9
- Lu N.Y., Helou G., Silbermann N. et al., in *ISO Conference: The Universe as seen by ISO*, p. 929
- Lutz D., Feuchtgruber H., Genzel R., et al., 1996a, *A&A* 315, L269
- Lutz D., Genzel R., Sternberg A., et al., 1996b, *A&A* 315, L137
- Lutz D., Spoon H.W.W., Rigopoulou D., Moorwood A.F.M., Genzel R., 1998, *A&A* 505, L103
- Madden S.C., Vigroux L., Sauvage M., 1997, in *XVIIth Moriond Astrophysics Meeting: Extragalactic Astronomy in the Infrared*, p. 229
- Madden S.C., Vigroux L., Sauvage M., 1999, in *ISO Conference: The Universe as seen by ISO*, p. 933
- Mathis J.S., 1990, *ARA&A* 28, 37
- Mattila K., Lemke D., Haikala L.K., et al., 1996, *A&A* 315, L353
- Mattila K., Lehtinen K., Lemke D., 1999, *A&A* 342, 643
- Moorwood A.F.M., Lutz D., Oliva E., et al., 1996, *A&A* 315, L125
- Mirabel I.F., Lutz D. & Maza J., 1991, *A&A* 243, 367
- Mirabel I.F., Vigroux L., Charmandaris V., et al., 1998, *A&A* 333, L1
- Mirabel I.F., Laurent O., Sanders D.B., et al., 1999, *A&A* 341, 667
- Murayama T., Mouri H., Taniguchi Y., 2000, *ApJ* 528, 179
- Murphy T.W., Soifer B.T., Matthews K., Kiger J.R., Armus L., 1999, *ApJ* 525, 85
- Ogasaka Y., Inoue H., Brandt W., et al., 1997, *MNRAS* 49, 179
- Oliva E., Moorwood A.F.M., Drapatz S., Lutz D., Sturm E., 1999, *A&A* 343, 943
- Onaka T., Yamamura I., Tanabe T., Roellig T.L., Yuen L., 1996, *PASJ* 48, 59
- Papoular R., Conard J., Giuliano M., Kister J., Mille G., 1989, *A&A* 217, 204
- Pier E.A. & Krolik J.H., 1992, *ApJ* 401, 99
- Puget J.L. & Léger A., 1989, *ARA&A* 27, 161
- Read A.M., Ponman T.J., 1998, *MNRAS* 297, 143
- Rigopoulou D., Spoon H.W.W., Genzel R., et al., 1999, *AJ* 118, 2625
- Risaliti G., Gilli R., Maiolino R., Salvati M., 2000, *A&A* in press (astro-ph/0002460)
- Roche P.F., Aitken D.K., Smith C., Ward M., 1991, *MNRAS* 248, 606
- Roussel H., Vigroux L., Sauvage M., 1999a, in *ISO Conference: The Universe as seen by ISO*, p. 957
- Roussel H., Vigroux L., Sauvage M., 1999b, *A&A* in preparation
- Sanders D.B., Mirabel I.F., 1996, *ARA&A* 34, 749
- Schulz B., Clavel J., Altieri B., et al., 1998, *ASP Conference Series* 146, 88
- Shlosman I., Frank J., Begelman M.C., 1989, *Nature* 338, 45
- Shlosman I., Begelman M.C., Frank J., 1990, *Nature* 345, 679

- Sloan G.C., Hayward T.L., Allamandola L.J., et al., 1999, ApJ 513, 65
- Smith H.E., Lonsdale C.J., Lonsdale C.J., 1998, ApJ 492, 137
- Soifer B.T., Neugebauer G., Matthews K et al., 2000, AJ 119, 509
- Starck J.L., Murtagh F., Pirene B., Albrecht M., 1996, PASP 108, 446
- Starck J.L., Murtagh F., Bijaoui A., 1998, Image Processing and Data Analysis, Cambridge University Press
- Starck J.L., Abergel A., Aussel H., et al., 1999, A&AS 134, 135
- Sturm E., Lutz D., Tran D., et al., A&A, in press (astro-ph/0002195)
- Terlevich R., Tenorio-Tagle G., Franco J., Melnick J., 1992, MNRAS 255, 713
- Tran D. 1998, PhD thesis, University of Paris XI, France
- Veilleux S., Kim D.-C., Sanders D.B., Mazzarella J.M., Soifer B.T., 1995, ApJS 98, 171
- Verstraete L., Puget J.L., Falgarone E., et al., 1996, A&A 315, L337
- Yun M.S., Scoville N.Z., Knop R.A., 1994, ApJ 430, 109

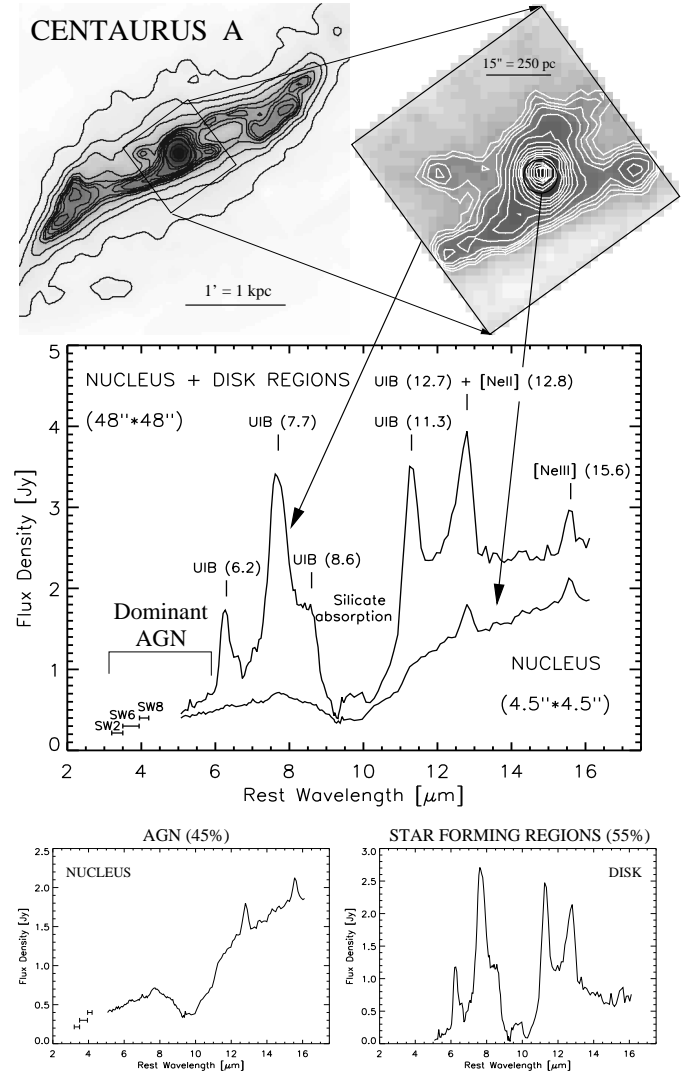


**Fig. 3.** Upper left panel : A  $7\ \mu\text{m}$  map of the dust emission in Cen A (from Mirabel et al. 1999). Upper right panel : The central region of Cen A as seen in the band  $7\text{--}8.5\ \mu\text{m}$  which traces the most intense UIB emission at  $7.7\ \mu\text{m}$ . Due to a good spatial resolution at  $7\ \mu\text{m}$  ( $\text{FWHM} = 5$  arcsec, i.e.  $100\ \text{pc}$  at  $3.5\ \text{Mpc}$ ), we can separate the nuclear region from the disk. Middle panel : The lower curve represents the MIR spectrum originating only from the nuclear region ( $100\ \text{pc}$  in diameter) whereas the upper curve shows the spectrum integrated over a larger region ( $800\ \text{pc}$  in diameter) which includes both disk structures and the nucleus. The silicate absorption cannot be well estimated from the global spectrum but is clearly detected in the AGN continuum. Lower panel : The AGN spectrum (left) represents 45% of the energy between  $5$  and  $16\ \mu\text{m}$  and it contributes more than 90% at wavelengths between  $3$  and  $6\ \mu\text{m}$ . No emission associated with star forming regions is detected between  $3\text{--}4\ \mu\text{m}$  (lower right panel, ISOCAM SW channel). While UIBs dominate the MIR emission of the disk, they are almost absent in a region of  $50\ \text{pc}$  radius around the AGN. The higher  $[\text{NeIII}]/[\text{NeII}]$  ratio detected in the AGN (lower left panel) further indicates the presence of a hard radiation field.

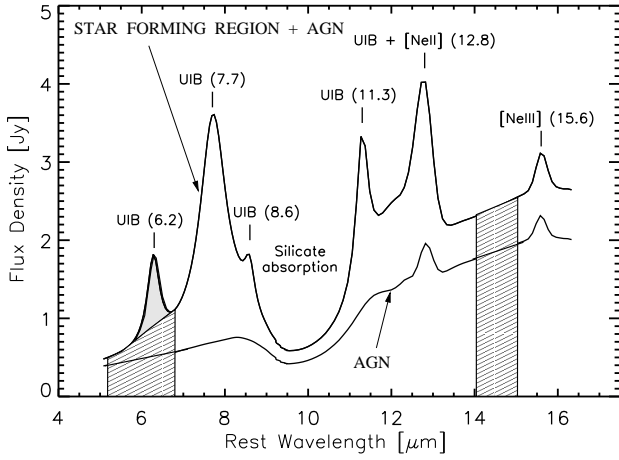


**Fig. 4.** The relative strength of the UIB( $6.2\ \mu\text{m}$ ) feature is estimated by dividing the spectrum between  $5.1$  and  $6.8\ \mu\text{m}$  in two different parts. One is the integrated flux above the line between  $5.9$  and  $6.8\ \mu\text{m}$  which is attributed to the UIB at  $6.2\ \mu\text{m}$  and traces essentially the PDRs in the star forming regions. The second is the integrated flux under the line which is mainly attributed to the AGN continuum and/or wing of the UIB at  $7.7\ \mu\text{m}$ . The feature to continuum indicator is used to estimate the relative contributions to the heating of the dust from quiescent star forming regions compared to the one from an AGN. We measure the “hot continuum” ( $5.1$ - $6.8\ \mu\text{m}$ ) which may contain an AGN contribution and compare it to the “warm continuum” ( $14$ - $15\ \mu\text{m}$ ) produced by both star forming regions and AGNs. As a consequence, the warm to hot continuum ratio can be used to quantify the relative contribution of a starburst continuum and an AGN in the MIR.

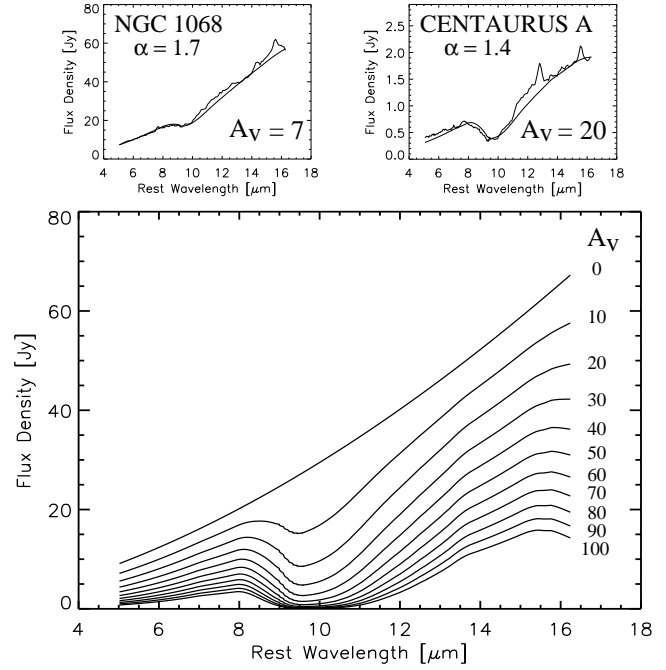


**Fig. 10.** The effects of absorption on AGN spectra characterised by a strong continuum at short wavelength associated with an absence of UIBs. In small panels, we display the nuclear spectra of NGC 1068 and CenA as well as a best fit based on a simple screen model (with the dust absorption law of Dudley & Wynn-Williams 1997) applied to a power law of spectral index  $\alpha$ . The corresponding visible absorptions for the fits are  $7$  and  $20$  mag respectively. The large diagram presents how the same power law spectrum ( $\alpha=1.7$ ) affected when absorption ranges from  $A_V=0$  to  $100$ .